Non conventional Imaging Systems for 3D Digitization of transparent and/or specular manufactured objects

Alban Bajard, Olivier Aubreton, David Fofi, Olivier Morel, Frederic Truchetet, Fabrice Meriaudeau

Non conventional Imaging Systems for 3D Digitization of transparent and/or specular manufactured objects

A. Bajard, O. Aubreton, D. Fofi, O. Morel, C. Stolz, F. Truchetet and F. Mériaudeau
Le2i Laboratory, UMR CNRS 6306
University of Burgundy
71200 Le Creusot, France
Corresponding author: fmeriau@u-bourgogne.fr

***Abstract*—3D scanning has been investigated for several years and most of the proposed approaches assume a diffuse or near diffuse reflectance of the object's surface, also called cooperative surfaces. For the case of "non cooperative surfaces", such as transparent objects or mirror-like surfaces, usually, a thin layer of powder is sprayed onto the object surface (to make it opaque and diffuse) prior to its digitization. This extra step is troublesome, time consuming (the object needs to be cleaned afterwards), and the final accuracy is often dependent on the powder thickness and its homogeneousness. To avoid this step, various methods have been investigated over the last few years. We propose in the paper to focus on three methods that we have been investigating over the last 10 years and compared their efficiency with those presented in the literature**

Keywords—3D Digitization, non diffused surfaces, Shape from polarization, Scanning from Heating, Shape from Induced Fluorescence.

I. INTRODUCTION

Machine vision systems which appeared in the industry 25 years ago have greatly benefited both from sensors evolution and from computing resources. Nowadays, systems measure all kind of parameters and rely on complex data such as multispectral information, polarization information as well as 3D information. These information are associated with high level image processing and powerful classification schemes led possible by the high computing power nowadays offered thanks to dedicated hardware platforms, graphical cards, clustered of PCs or even cloud computing. However, while machine vision capabilities were improving, design and productions followed the same trend leading to more fashion and more complex products, creating the need to develop systems able to control the 3D aspects of complex (in shape and in composition) objects. 3D scanning has been investigated for several years and most of the proposed approaches assume a diffuse or near diffuse reflectance of the object's surface. The broad literature on the subject is usually divided into active and passive techniques. Active light techniques, whose a recent review is proposed by Blais [1], include laser range scanning, coded structured light systems, digital holography and time-of-flight scanners whereas passive techniques are mainly stereovision, shape-from-X (shading, optical flow, motion, focus, defocus…).

For the case of "Non Lambertian objects", such as transparent objects or mirror-like surfaces, usually, a thin layer of powder is sprayed onto the object surface (to make it opaque and diffuse) prior to its digitization. This extra step is troublesome, time consuming (the object needs to be cleaned afterwards), and the final accuracy is often dependent on the powder thickness and its homogeneousness.

To avoid this step, various methods have been investigated over the last few years. An exhaustive and recent review can be found in [2] which was further completed by Meriaudeau et al. [3] for the case of transparent objects. Also, the recent paper of Osorio et al. released in 2012 [4] presents a thorough literature review and an original technique which relies on multi-wavelength range sensing which is very similar to the shape from induced fluorescence [5] which will be presented later on. Most of the presented methods : shape from distortion [6], light path triangulation [7], scatter trace photography [8], Phase-shift method [9], visible tomography [10], Multipeak range imaging [11], polarisation [12], polarisation and phase shifting [13], specular flow [14], immerse light projection associated with fluorescence [15],.... which originally come from the computer graphics community, require some a priori about the object or assumptions about the interactions of the light with the object surface and are not yet ready to be implemented in the industry. This paper presents some of our recent work, including shape from induced fluorescence [5], scanning from Heating [16-17] with an extension to metallic objects, as well as shape from polarization [18] with a multispectral extension [19] and to compare them to the most relevant technique presented in [2] and [3]. For each aforementioned technique, our paper also presents videos illustrating on-line scanning of non conventional objects.

The rest of this paper will therefore consist of four different parts and is organized as follows: the first part will present focus on the scanning from heating. After presenting the theory beneath the method, results obtained in the case of specular objects and transparent objects will be displayed. The second part will be devoted to the shape from polarization technique. After presenting the general aspects, highlighting the weaknesses of the original method [12], we will present various options so as to remove the ambiguities on the

azimuthal and zenithal angles, enabling the system to be used for transparent [18] as well as metallic objects [19]. The last method later called “shape from induced fluorescence” will be presented in the third part. The concept and two different methods of active scanning by mean of a line or a point will be presented. 3D reconstructions of transparent objects made of glass or plastics will be presented. For these three methods, deviation maps between golden standard obtained with a commercial active lighting scanner or a touch probe scanner and our systems will be presented so as to assess the accuracy of each method.

In the fifth part, we will attempt to conclude and classify each of the presented techniques using criteria such as time complexity, calibration requirements, equipment cost, accuracy, versatility, a priori needed, possible on-line implementation within an industrial environment.

II. Scanning From Heating

To address the problem of 3D acquisition of optically challenging surfaces such as polished metallic objects, glass objects or plastic objects, we propose a non-conventional infrared approach. In the field of 3D digitization, thermal images are rarely used. Nonetheless, in the field of non-destructive testing, some “active thermography” techniques can be found in the literature; for example, Bodnar and Egee [25] shows how to detect cracks in metallic materials due to wear. Thanks to a moving photothermal probe, they propose to approximate the dimensions of the crack according to a prior theoretical classification. The first research studies to consider thermography to extract complete 3D information were conducted by Maldague and Pelletier [26], [27] the technique is called “Shape from Heating” and its first goal is to improve the detection of sub-surface defects by pulsed thermography. In the 3D shape approximation stage (the accuracy is not evaluated), the thermograms can be corrected by removing the temperature variations resulting from the non-planarity of the surface. More recently, some researchers took an interest in combining temperature measurements and 3D shape reconstruction by implementing a stereovision system in the far infrared spectral band [28], [29] or the near infrared [30]. However, the difficulty to extract features for dense matching from stereo images is still an open problem [31].

The work presented in the following part of the paper is a method that unifies 3D digitization abilities on optically non-cooperative surfaces: the Scanning From Heating (SFH) [16], [17], [35].

A. Working Principle

The principle of this technique is different from standard active triangulation technique in the sense that we measure the thermal radiation emitted from a heated point instead of acquiring the reflection of a visible light pattern on the surface. Assuming that infrared emission distribution is omnidirectional for most materials, we can deal with specular or even refractive surfaces, regardless of the scanner position. To do the digitization, an infrared laser source is geometrically calibrated with a thermal sensor to extract a cloud of 3D points from infrared images. If the wavelength of the laser source is correctly selected, the technique can be applied either on transparent surfaces or on specular surfaces. For example, radiative behavior of glass objects tends to be similar to opaque ones if the incident wavelength is above 10 µm (no transmission). For specular metallic objects, incident radiation should belong to the near infrared spectral band, because absorptivity values are higher and thermal emission can occur. In both cases, since the emission of infrared radiation is omnidirectional, the acquisition of a point is not limited when the surface gradient is high. This aspect was still an open problem for reflection-based scanners when acquiring a non-Lambertian surface.

Knowing the thermophysical properties of common materials, we have built a theoretical model of heat exchanges induced by the technique. The energy balance is evaluated for the three exchange modes that are: conduction, convection and radiation. We finally obtain partial differential equations that are solved in 3D using a finite element numerical solver. The simulation results [35] help to validate the feasibility of the technique on dielectric or metallic materials and to predict the best settings of the system (incident power, pulse time) for a given surface. Indeed, the generated heated point has to be intense enough to be detected by the sensor but it should not exceed a temperature limit, which would lead to damaging the surface by melting or marking. According to the computations on materials that are commonly used in industry, two experimental devices are proposed for each category of challenging surfaces: transparent and specular ones.

B. Experimental Setups

A first SFH-based prototype has been implemented in order to handle specular metallic objects digitization. To demonstrate the feasibility of our method, a first system was mounted on a 3-axis moving table [35] but the scanning process was particularly long and the optical quality of the laser beam was not sufficient. In order to avoid mechanical vibrations and increase the accuracy of the scanning, a novel system was designed (see figure 1). In particular, a galvanometer scan head is inserted; it reduces significantly the dimensions of the system and improves the scanning speed and quality thanks to two mirrors. The different parts of the experimental setup are described below.

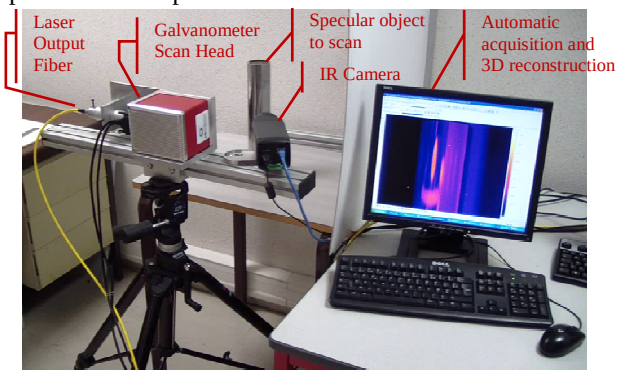

Figure 1 – Photo of the scanner prototype

The fiber laser source emits at 1.07µm and its power ranges from 0 to 50W. Concerning the choice of the incident wavelength, we can rely on the numerous databases of optical

constants in the literature ([10], [11]). Indeed, the absorption coefficient of metallic surfaces tends to increase when the wavelength decreases, that is why the laser wavelength should be chosen in the near infrared spectral band. The optical components are three lenses that are assembled through the laser optical path, focusing the laser to a 0.44mm beam waist at 500mm with a 200mm depth of field. The galvanometer scan head is made up of two mirrors deflecting the laser beam with 150µrad step. The IR camera contains a bolometer detector, sensitive to Long-Wavelength ([8-13] µm).

In order to deal with transparent surfaces, a second setup has been designed. The basic structure of the system is similar to the previous one, but some significant differences have to be noted. The X-Y translation is realized with a moving platform. This system is slower than the galvanometer mirrors but is able to reconstruct larger objects up to 80×150×30cm. The heating source is a CO_2 laser and emits radiation at 10.6 µm, with a maximum power of 400mW. The quantity of energy is enough to heat a dielectric surface since its emissivity value is extremely higher than for metallic ones. The spectral band of sensitivity of the IR camera is different from the system described above. The laser wavelength should not be included in this band so that neither direct laser radiation nor reflection can be detected. Consequently, the used detector is sensitive to MW band ([3-5] µm).

C. Calibration method

Before the acquisition step, it is necessary to geometrically calibrate the laser-camera system. The systems that are described in the last section use the same calibration principle. In the following part, we detail the calibration method for the galvanometer based system. Because the Rayleigh length of the laser (equivalent to the depth of field) is relatively long, we assume that there is no geometrical aberration, so the laser calibration is only based on the calculation of its extrinsic parameters, i.e. two rotations that are given by each galvanometer mirror. The electrical signals that command the mirror motors are linearly related to the deflection angles α_x and α_y. The experimental determination of this relation is performed to know the position of the laser beam that is used for the scanning process.

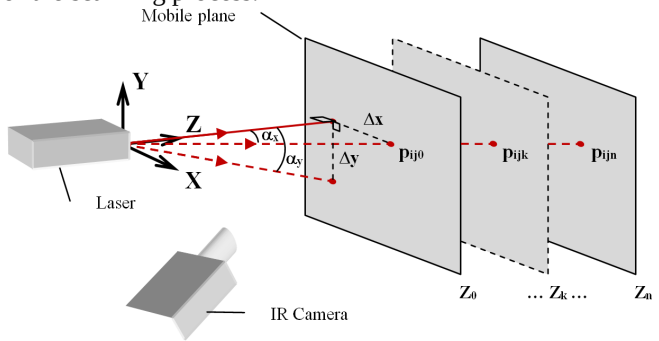

Figure 2 – Calibration method

The world frame is attached to the rotation center of the galvanometer scan head. After laser calibration step, we have to compute the transformation between the world frame and the image frame. The principle of the method we have implemented [34] is based on the rules of projective geometry. As illustrated in figure 2, a calibration plane is translated along *Z* direction, perpendicularly to the laser incidence direction. For each known position *(i,j)* of the beam, the plane is translated into *k* positions in Z (at least three) within the desired measurement zone, describing *k* intersection points p_{ijk}. For each sampled position of the laser ray, five calibration parameters are computed. The first two parameters are the coefficients a_{ij} and b_{ij} of the equation of the straight line Δ_{ij} described by the points p'_{ijk}, which are the corresponding points of p_{ijk} in the image projection frame. Then the relative position *D* in pixels of every point is computed on each line Δ_{ij}:

$$D_{ijk} = \left\| p'_{ijk} - p'_{ij0} \right\| \quad (1)$$

with p'_{ij0} the corresponding 2D point of the intersection between the laser beam at *(i,j)* position and the plane at the first position Z_0.

One can demonstrate that the relation between the coordinate Z_k and the distance D_{ijk} is given by the following:

$$Z_k = \frac{c_{ij} D_{ijk} + d_{ij}}{e_{ij} D_{ijk} + 1} \quad (2)$$

where c_{ij}, d_{ij}, e_{ij} are the three others parameters of the calibration.

Knowing these five parameters and the angle position of the beam (α_i,α_j), we can compute the three world coordinates of the considered point p_{ijk} from the 2D coordinates of its corresponding point p'_{ijk} in the image frame. The point p'_{ijk} is localized in the image frame after several successive steps of image analysis: background substraction (based on the image acquired before the laser pulse), gaussian filter, segmentation of the heated spot (based on region growing around the intensity maximum), subpixellic computation of the central point of this spot, and orthogonal projection of this point on the corresponding line Δ_{ij}. This stage is iteratively repeated for each position of the laser beam to scan the whole surface of the object to be digitized.

D. Results and discussions

1) Metallic materials

Experiments were conducted on different materials (specular or not) with various geometries. Results presented in figure 3 are obtained with a scanning window of 1600 points (40rows×40columns). The laser beam orientations are regularly spaced by 0.3 deg. The incident laser power chosen for the four examples is respectively 6W, 20W, 25W and 10W and the pulse duration is 100ms. An example of the measurement accuracy can be given by the estimation of the cylinder diameter from the fitted surface to the 3D cloud of points: our result is 67.899mm whereas the reference diameter measured by a touch-probe scanner is 68.001mm, which means that the error is only 102µm. Concerning the example of the spoon, a comparison has been computed between the points that were acquired by the SFH-based scanner and a reference cloud of points measured with a commercial scanner on the powdered surface. The average distance is 143µm and the standard deviation of the error distribution is 178µm. The

error is mainly localized on the edges, where the sampling step of the scanning is not narrow enough. The work presented in [35] gives a detailed evaluation of the performance of the technique by introducing a comparison with a conventional 3D acquisition system. It also highlights the main contribution of SFH application to metallic surfaces: unlike other existing techniques of acquisition that are based only on the interpretation of specular reflection of visible light, our technique can operate with similar accuracy on diffuse and specular surfaces, in other terms the performance no longer depends on the roughness of the surface.

2) Dielectric materials

To prove the versatility of the Scanning From Heating method, digitization tests have been performed on several transparent objects (see [36] for further details). Some of them are presented in figure 4. As shown in the two first results, the feasibility has been validated for complex transparent glass objects. To quantify the digitization accuracy, we compare our results to the models generated by conventional scanner from the powdered surface. For a set of five glass objects of this category, the average deviation ranges from 150 µm to 360 µm. Figure 4 shows that it is also possible to apply the method to plastic material. The plastic bottle has been reconstructed with an average deviation of 200 µm.

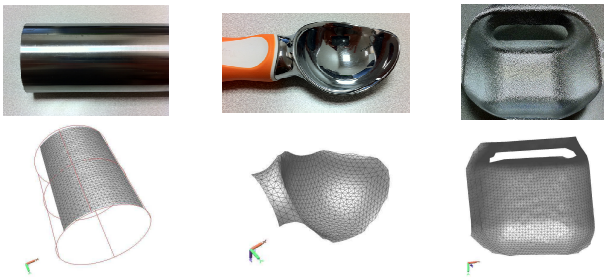

Figure 3 – 3D Digitization results obtained by SFH on metallic surfaces

Figure 4 – 3D Digitization results obtained by SFH on transparent surfaces

III. SHAPE FROM POLARIZATION

A. Background

In the early 1990s, cameras able to recover the information based on the polarization state of the light, were emerging. Wolff [20-21] was one of the pioneers when designing a polarimetric camera with applications dedicated to material identification and separation of diffuse and specular components in the observed scene. Afterwards, Rahmann [22-23] and Saito [24] showed the possibility to link polarimetric parameters to depth in the observed scene leading to the new concept of "shape from polarization", and establishing a bridge with the earlier theory developed by Horn [37] in the context of "shape from shading". The aim of the shape from polarization technique is to measure the normal at each point and then to obtain the whole surface by integration of the normals field. The shape from polarization was applied by Miyasaki et al. [38-40] and Ferraton et al. [19] for transparent objects and by Morel et al. [18] for their metallic counter parts. The two later ones, emerging from our research group, are presented thereafter.

B. Shape from polarization principle

The principle of polarization imaging relies on the following principle: after reflection, a non-polarized light wave becomes partially linearly polarized according to the normal to the surface and the optical index of the material at the point of incidence. A partially polarized wave may be defined by three parameters which are: the light intensity I, the degree of polarization ρ and angle of polarization φ. The two latest parameters are respectively linked to zenithal angle θ and the azimuthal angle ϕ through the Snell-Descartes relations. Therefore measuring the degree of polarization ρ and angle of polarization φ enables to infer the normal at each point by means of the zenithal angle θ and the azimuthal angle ϕ. This normal field is then integrated to recover the 3D shape of the object. The study of the state of polarization of a light wave requires a rotating polarizer placed in front of an orthographic camera or a combination of active components acting as a rotating polarizer [41]. The relationship between the measured intensity I_p, the total light magnitude I_{tot}, the polarization angle φ and the orientation angle α of the polarization filter is given by:

$$I_p(\alpha) = \frac{I_{tot}}{2}(\rho\cos(2\alpha - 2\varphi) + 1) \tag{3}$$

where the degree of polarization is defined by:

$$\rho = \frac{I_{\max} - I_{\min}}{I_{\max} + I_{\min}} \tag{4}$$

And it is equal to zero when the light is not polarized and equal to 1 when the light is linearly polarized which corresponds to the incident angle equal to the Brewster angle. Equation (3) can also be written as:

$$I_p(\alpha) = \frac{1}{2}(S_0 + S_1\cos 2\alpha + S_2\sin 2\alpha) \tag{5}$$

where S_0, S_1 and S_2 are the unknown Stokes parameters [42] expressed as:

$$\begin{aligned} S_0 &= I_{tot} \\ S_1 &= \rho I_{tot}\cos 2\varphi \\ S_2 &= \rho I_{tot}\sin 2\varphi \end{aligned} \tag{6}$$

The purpose of the polarization imaging is to calculate I_{tot}, ρ and φ through formulas (3) and (4) or (5) and (6). We used the second solution, by taking 18 images with the polarizer turned of 10° between each acquisition, and solve the system using least mean squares. This solution is more robust against noise compared to the evaluation of the parameters through

equations (3) and (4). The Fresnel formulae that provides relationship at media interface between incident, reflected and refracted light show that the azimuth angle ϕ can be inferred from the angle of polarization φ:

$$\phi = \varphi \pm \frac{\pi}{2} \quad (7)$$

In other words, the reflected light is linearly partially polarized orthogonally to the incidence plane. This equation raises an ambiguity that can be solved by using an active lighting as presented by Morel et al. [18].

C. Applications

1) Applications to metallic surfaces

The "Shape from Polarization" method was successfully extended to specular metallic surfaces in [18]. The main point is that the refractive index of metallic object is complex and the relationship between the degree of polarization ρ and the zenith angle θ is different from what was found by Myasaki et al. [40]. Indeed, the following approximation is required to simplify the equation:

$$|\hat{n}|^2 = n^2(1+\kappa^2) \gg 1 \quad (8)$$

The relation is valid in the visible case [43] and enables to obtain:

$$\rho(\theta) = \frac{2n\tan\theta\sin\theta}{\tan^2\theta\sin^2\theta + |\hat{n}|^2} \quad (9)$$

The difference between the true degree of polarization and its approximation is insignificant. The function given by the relation (9) is bijective for metallic surfaces, when θ is lower than 80°. Since for most objects, slopes are lower than 80°(continuous surfaces with smooth slopes), there is no ambiguity concerning the determination of the angle θ, according to the degree of polarization ρ ; contrary to dielectrics (this aspect will be tackled later on for transparent objects).

a) Acquisition setup

The acquisition system is made of a CCD camera, a liquid crystal polarization rotator, and an active diffuse dome light (figure 5). The active diffuse dome light is used both to provide an unpolarized light on the whole surface and to solve the ambiguity concerning the azimuth angle. Since the target object is highly specular, it is placed in the center of the dome to be illuminated on most part of its surface. After reflection the light which becomes partially linearly polarized is analyzed with the liquid crystal polarization rotator and the camera. The liquid crystal polarization rotator acts like a rotating polarizer, which can electrically be controlled.

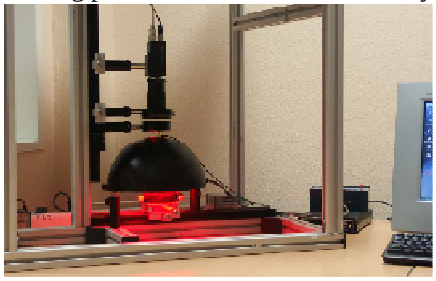

Figure 5 – Experimental setup

This device uses nematic liquid crystal cells associated with a linear polarizer, and a quarter wave plate, which provides tunable polarization by changing the supplied voltage. The proposed system is therefore fully automatic and it takes 7.5 seconds to get a 1024×1024 height image.

b) Results

The three-dimensional reconstruction of surfaces is linked to the acquisition system accuracy and to the object shape. Thus, instead of comparing the shape reconstructed from different devices, the normals of calibrated spheres were compared. A perfectly specular metallic hemisphere, with a refractive index equaled to $\hat{n} = 1.94 + 5.28i$, was used with the polarimetric system whereas a mat hemisphere was used with the two based on triangulation: the Replica 500 scanner and the MinoltaVI-910 scanner. It was found that the error from the polarimetric system is quite random and homogeneous on the surface except on the center, where the normals are oriented near the optical axis. It is both due to the hole in the dome and to the degree of polarization that becomes very small in this region. Indeed, in this case the reflection coefficients are nearly the same, increasing slightly an uncertainty concerning the angle ϕ. Table 1 presents the normals mean error with $\theta_r \in [0,80°]$ for two different size hemispheres and shows the good accuracy of the polarimetric system to compute the surface normals.

Table 1 – Mean error on normals acquisition

Sphere diameter	Pola. system	Replica	Minolta
41.275 mm	0.0695	0.0882	0.1034
44.450 mm	0.0644	0.0614	0.0790

The three-dimensional inspection of highly reflective metallic surfaces remains a delicate task in industrial vision. Many systems exist and are efficient to discriminate geometric aspect defects [44] but unfortunately they can't provide 3D shape information that is essential to reveal the shape defects on decorations from metallic objects made by stamping and polishing (figure 6-(a)). With the polarimetric system, the three-dimensional surface of a reference object is computed by shape from polarization. The three-dimensional surface of the objects to be inspected are also computed and compared to the reference one. After registering the two shells, the mean deviation between the surfaces is computed (figure 6-(b)) and the shape defects can be efficiently discriminated.

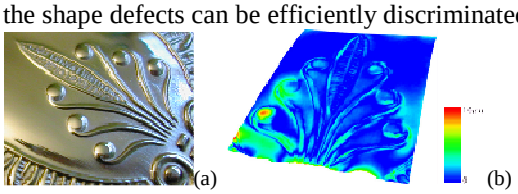

(a) (b)

Figure 6 – Three-dimensional inspection of specular defects by polarization imaging: (a) photograph of the object, (b) deviation map computed from Shape from Polarization

2) Transparent surfaces

a) Background

As presented earlier, the concept of shape from polarization, that proved to work well for metallic surfaces, was first introduced for transparent ones [12]. In this case due to the lower value of the Brewster angle, some assumptions

have to be made in order to leave this ambiguity since the curve of the degree of polarization is not bijective. A first approach was based on image segmentation [45] where the whole object is in the field of view and spatial relationships within pixels and initial guess (or knowledge) of the slope is propagated in the algorithm. Another approach consists in applying a slight tilt to the object and measure the variation (first derivative) of the degree of polarization in respect of the zenithal angle [38]. A final approach introduced by Myasaki et al. [40] consists in a double measure of the degree of polarization: one in the visible and one in the infrared domain of the spectrum. However the method, if proved to work, requires from a practical point of view the use of two setups: one in the IR, one in the visible. The setup in the IR implies to heat the object and to observe the emitted wave (due to thermal radiation) by using an adapted IR sensor sufficiently sensitive. A strong assumption is therefore needed on a homogenous temperature of the object so as to avoid any dependency on the wavelength of the radiated (thermal) wave.

b) A multispectral solution

At the contrary, a more general concept based on the wavelength dependent shift of the curve of the degree of polarization can be introduced [19]. At two distinct wavelengths the curve of the degree of polarization versus θ, are crossing near the Brewster angle (see figure 7-a). If measured accurately, these information can enable to infer the degree of polarization and remove the ambiguity on the zenithal angle θ [46]. This was done thanks to the availability of electrically controlled retarders that can be finely tuned thanks to a proper calibration procedure. The polarization state of the reflected light is studied through the use of a prototype composed of several elements: a color dome light wavelengths (472nm, 513nm and 655nm) to control the lighting conditions and illuminate the object with a non-polarized light; on optical analyzer composed of a combination of an electrically controlled liquid crystal variable retarder (LCVR), a polarizer and a quarter wave plate. The method proposed by Ferraton et al. [19] uses a Saliency operator to detect the appropriate voltage necessary to assume proper polarimetric rotation. The calibration was performed for the three wavelengths and the results on a sphere where the slope can provide reflection beyond the Brewster angle shows the feasibility of the approach (figure 7). We have also recently reported a nice extension of this method in the mid-IR range (9 µm) [47].

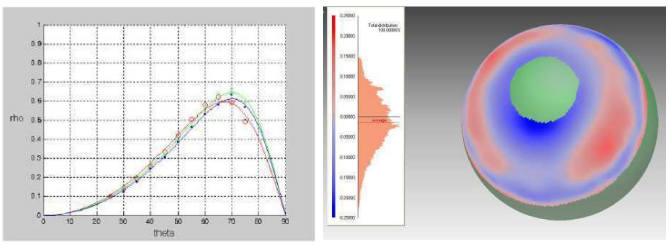

(a) (b)

Figure 7 – (a) Average degree of polarization recorded for different plate tilt for the three wavelengths and complex index estimation. (b) Reconstruction of a sphere object and deviation map.

IV. Shape From Induced Fluorescence

A. Background

The novelty of the proposed approach lies in the exploitation of the fluorescence generated at the object surface under the irradiation of a UV Laser using a specific triangulation approach associated with a fluorescence points tracking method [5]. A similar approach with the tuning of a commercial scanner was recently proposed by Osorio et al [4].

B. Fluorescence points tracking method

A tracking approach based on fluorescence intensity modelling has been carried out to perform the fluorescence point extraction algorithm in the presence of noises. Indeed, some inter-reflection (figure 8) induced by the observed visible fluorescence light perturbed the identification and the localization of the fluorescence point. Represented in any shape, noises are mainly caused by the incident angle of the excitation UV ray (thus related to the object's shape) with an intensity which is more or less accentuated by the object's properties. The emission spectrum specific to each considered application material [5] led us to model the fluorescence point intensity using Gaussian distribution to deal with noises.

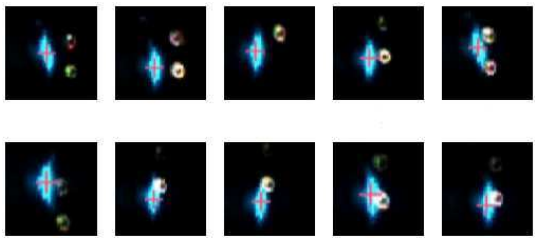

Figure 8 – Zoom of the tracked fluorescence points

Therefore, the fluorescence tracking is done in two steps for each analyzed image:

- A basic global threshold is first applied on the image in order to segment pixels of high intensity in the channel when the highest emission is expected
- The thresholded pixels's RGB components are then used to verify the Mahalanobis distance criterion as in equation (10). The intensities of pixels representing the laser fluorescence are preliminary modelled by a Gaussian distribution for each considered scanned material. Considering RGB space, its distribution (*k*) is characterized by a mean vector μ_k and a covariance matrix Σ_k related to the intensities of a given class of the material fluorescence. Gaussian parameters are learned from few training images. Hence, to track the fluorescence spot for a material (*k*) which Gaussian parameters are defined, one verified that for each given pixel if its intensity I satisfies the inequality expressed below:

$$D_M(I) = \sqrt{(I-\mu_k)^T \Sigma_k^{-1} (I-\mu_k)} \leq T_k \qquad (10)$$

Where D_M is the Mahalanobis distance for a given intensity I towards a considered class of distribution (*k*) and T_k a threshold defined by the maximum Mahalanobis distance calculated from the training data used to estimate the Gaussian distribution parameters. Consequently, all pixels satisfying the

inequality (10) correspond to the fluorescence spot (k) and the centroid spot pixels whose intensity's value are the highest is computed to select the representative fluorescence point to be reconstructed. Figure 8 is an example of the tracking results.

C. Experimental setup and results

a) Transparent objects

The initial practical setup (figure 9) is composed of a fixed UV laser (266 nm) associated with a fixed classical visible RGB CCD camera. Under UV irradiation, the transparent surface emits a visible light in a diffused manner due to the induced fluorescence. Bright spots (width estimated size ~4×2 mm on a flat surface) are then imaged by the camera and used to estimate the object's depth according to a triangulation approach from a structured light source identical to the one presented in the Scanning from Heating section. During the acquisition, the object to be digitized is placed on a translation table (MM4005 4-axis Motion Controller/Driver: Newport, which offers accurate horizontal and vertical displacements (the error is never greater than 2% for a 1µm motion). Thus, (X Y) 2D coordinates are preliminarily defined (translation of the table) while the depth Z is to be estimated by the triangulation scheme. Results on more than 10 different objects of various shapes, various materials (glass, plastic...), and various thicknesses were reported [5].

Figure 9 – Experimental configuration for the point scanning approach

While comparing our measurements with those either obtained with a commercial scanner (once the objects are being coated with a diffuse coating layer), the mean deviation error can be as low as 100 µm (see figure 10) showing the high accuracy and the huge potential of this new method (as also demonstrated by Osorio et al. [4]). On the other hand, the accuracy is highly affected by the number of sampling points (the displacement of the object through the translation table) and therefore highly affects the time needed to fully scan the object. We have also proposed an extended version to generate a line scanner by inserting a hemi-cylindrical lens within the beam, which is aimed to reduce the acquisition time as well as the processing time.

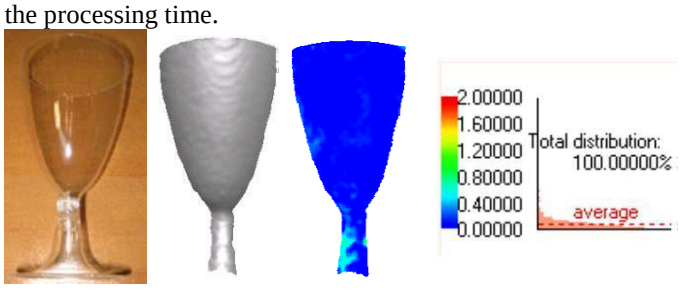

(a) (b) (c)

Figure 10 – (a) Original plastic glass, (b) plastic glass digitized with our method, (c) associated error map

b) Metallic objects

Using the point scanning approach, encouraging preliminary results were obtained on highly specular aluminum objects (see figure 11). We are currently investigating further metallic objects in order to fully validate the method.

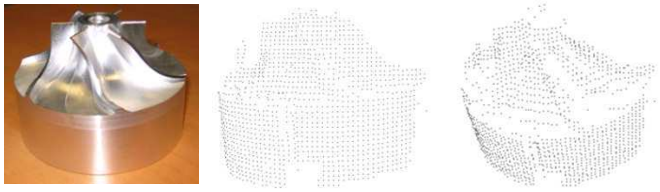

(a) (b)

Figure 11 – (a) Original metallic (aluminum) surface, (b) 3D data cloud obtained with the point scanning method

V. CONCLUSION

Table 2 summarizes the pros and cons of all techniques either presented here or in the references [2], [3] and [4]. The shape from induced fluorescence [5] or the similar approach proposed by Osorio et al. [4] provides good, versatile and accurate results. It offers the greatest potentiality for industrialization. The Scanning from heating, apart from the cost, has proven to be reliable and accurate for both transparent and specular surfaces. Whereas Shape from polarization gave good results for highly reflective objects, its extension to transparent surfaces is still at the laboratory stage due to the tedious calibration of all the optical components; however its extension in the infrared spectrum [47] seems very promising and should therefore be fully investigated. It has to be noted that accurate results for complex transparent objects were also obtained by Hullin et al. [15] but the immersion phase prevents this method to be implemented with the industry.

Table 2 – Comparative table of different digitization techniques on non-cooperatives surfaces

	Accuracy	Cost effective	Possible online application	No a priori needed	Complex objects	No need for high post-processing	Versatility	References
Shape from Induced Fluorescence or multi-wavelength range imaging	✓	✓	✓	!	✓	!	!	[4], [5]
Scanning from Heating	✓	✗	✓	!	✓	!	✓	[16], [17], [35]
Shape from Polarization	!	!	!	✗	!	!	!	[18-19], [37-40],[46-47]
Shape from Distorsion	✓	✓	✗	✗	!	✗	✓	[6],[15]
Light Path Triangulation	!	✓	✗	✗	✓	✗	✗	[7]
Shape from Tomography	!	✗	✗	✗	!	!	✗	[10]
Polarization and phase shifting	!	✓	✗	✗	!	✗	✗	[13]
Multipeak range imaging	!	!	✗	✗	✗	✗	✗	[11]

✓ Optimal
! Good
✗ Not so good

VI. REFERENCES

[1] F. Blais, Review of 20 Years of Range Sensor Development, Journal of Electronic Imaging 13, 1,pp. (231–243, (2004).

[2] Ihrke, Kiriakos N. Kutulakos, Hendrik P. A. Lensch, Marcus Magnor, Wolfgang Heidrich , Transparent and Specular Object Reconstruction , Computer Graphics Forum, Vol. 29, number 8 pp. 2400–2426, (2010).

[3] F. Mériaudeau, R. Rantoson, D. Fofi, C. Stolz ,“Review and comparison of Non Conventional Imaging Systems for 3D Digitization of transparent objects”, Journal of Electronic Imaging , 21(2), 021105 (Apr–Jun 2012).

[4] M. F. Osorio, A. Salazar, F. Prieto, P. Boulanger, and P. Figueroa, "Three-dimensional digitization of highly reflective and transparent objects using multi-wavelength range sensing," Machine Vision and Applications, vol. 23, no. 4, pp. 761-772, (2012.)

[5] R. Rantoson, C. Stolz, D. Fofi and F. Meriaudeau, “Optimization of Transparent Objects Digitization from Visible Fluorescence UV-induced Optical Engineering”, Optical Engineering, 51(3), 033601 (March 2012).

[6] M. Tarini, H. Lensch, M. Goesele, H-P Seidel , "Shape from distortion: 3D range scanning of mirroring objects", Proceeding SIGGRAPH '02 .

[7] E. Steger and K. N. Kutulakos," A Theory of Refractive and Specular 3D Shape by Light-Path Triangulation". Int. J. Computer Vision, vol. 76, no. 1, pp. 13-29, (2008).

[8] N. J. W. Morris and K. N. Kutulakos, reconstructing the surface of inhomogeneous transparent scenes by scatter-trace photography, in Proc. IEEE 11th ICCV, pp. 1–8, (2007).

[9] M. Yamazaki, S. Iwata, G. XuIn Y. Yagi “Dense 3D Reconstruction of Specular and Transparent Objects Using Stereo Cameras and Phase-Shift Method”,. ACCV 2007, Part II, LNCS 4844, pp. 570–579, 2007.

[10] B.Trifonov, D. Bradley, W. Heidrich, Tomographic Reconstruction of Transparent Objects, Eurographics Symposium on Rendering, Tomas Akenine-Möller and Wolfgang Heidrich (Editors), (2006).

[11] J. Park and A. C. Kak, “3-D modeling of optically challenging objects,” IEEE Trans. Vis. Comput. Graphics. 14(2), 246–262 (2008).

[12] M. Saito, Y. Sato, K. Ikeuchi, and H. Kashiwagi, “Measurement of Surface Orientations of Transparent Objects by Use of Polarization in Highlight" , J. Opt. Soc. Am. A, 16, (9), pp. 2286-2293, (1999).

[13] T. Chen, H. Lensch, C. Fuchs and H-P Seidel. "Polarization and Phase-shifting for 3D Scanning of Translucent Objects". IEEE Computer Society Conference on Computer Vision and Pattern Recognition (CVPR 2007), Minneapolis, Minnesota, USA, June 18-23, (2007).

[14] S. Roth, M.J. Black, "Specular Flow and the Recovery of Surface Structure", In Proc. of the IEEE Conference on Computer Vision and Pattern Recognition (CVPR), vol. 2, pp. 1869-1876, (June 2006).

[15] M. B. Hullin, M. Fuchs, I. Ihrke, H.-P. Seidel, and H. P. A. Lensch, (2008) , Fluorescent immersion range scanning, in ACM Trans. Graphics, vol. 27, no. 3, pp. 87:1–87:10.

[16] G. Eren, O. Aubreton, F. Meriaudeau, L. A. Sanchez Secades, D. Fofi, A. T. Naskali, F. Truchetet, and A. Erçil, "Scanning From Heating : 3D shape estimation of transparent objects from local surface heating," Optics Express, vol. 17, no. 14, pp. 11457-11468, (2009).

[17] F. Meriaudeau, L.A. Sanchez-Secades, B. G. Eren, B. A. Erçil, F. Truchetet, A. O. Aubreton, and D. Fofi , “3D Scanning of Non-Opaque Objects by means of Infrared Imaging”, IEEE On Transaction on Instrumentation and Measurement, 59 (11), pp. 2898-2906, Nov. (2010).

[18] O. Morel, C. Stolz, F. Meriaudeau, and P. Gorria. Active lighting applied to 3d reconstruction of specular metallic surfaces by polarization imaging. Applied Optics, 45(17):4062–4068, (June 2006).

[19] M. Ferraton, C. Stolz, F. Meriaudeau “Optimization of a polarization imaging system for 3D measurements of transparent objects”, Optics Express, Optical Society of America, 17 (23), pp. 21077-21082, (2009).

[20] L. B. Wolff. Polarization-based material classification from specular reflection. IEEE Trans. Pattern Analysis and Machine Intelligence, 12(11):1059–1071, (November 1990).

[21] L. B. Wolff and T. E. Boult. Constraining object features using a polarization reflectance model. IEEE Trans. Pattern Analysis and Machine Intelligence, 13(7):635–657, (July 1991).

[22] S. Rahmann, "Polarization images: a geometric interpretation for shape analysis," in IEEE International Conference on Pattern Recognition (ICPR), pp. 542-546, (2000).

[23] S. Rahmann, "Reconstruction of Quadrics from Two Polarization Views," in Iberian Conference on Pattern Recognition and Image Analysis (IbPRIA03), (Springer, 2003), pp. 810-820, (2003).

[24] M. Saito, Y. Sato, K. Ikeuchi, and H. Kashiwagi, "Measurement of Surface Orientations of Transparent Objects Using Polarization in Highlight," in IEEE Conference on Computer Vision and Pattern Recognition, pp. 381 – 386, (1999).

[25] J.L. Bodnar and M. Egée, "Wear Crack characterization by photothermal radiometry," WEAR, vol. 196, pp. 54-59, (August 1996).

[26] X. Maldague, Barker E., A. Nouah, E. Boisvert, B. Dufort, and L. Fortin, "On Methods for Shape Correction and Reconstruction in Thermographic NDT," in IInd International Workshop on Advances in Signal Processing for NDE of Materials, Kluwer Academic Pub., Québec, QC, pp. 209-224, (1994).

[27] J-F. Pelletier and X. Maldague, "Shape from heating: a two-dimensional approach for shape extraction in infrared images," Optical Engineering, vol. 36, no. 2, pp. 370-375, (February 1997).

[28] S. Prakash, P. Y. Lee, and T. Caelli, "3D Mapping of Surface Temperature Using Thermal Stereo," in 9th International Conference on Control, Automation, Robotics and Vision, Singapore, pp. 1-4, (2006).

[29] B. Ducarouge, "Reconstruction 3D infrarouge par perception active," INSA Toulouse, Toulouse, PhD thesis, 2011.

[30] J.-J. Orteu, Y. Rotrou, T. Sentenac, and L. Robert, "An Innovative Method for 3-D Shape, Strain and Temperature Full-Field Measurement Using a Single Type of Camera: Principle and Preliminary Results," Experimental Mechanics, vol. 48, no. 2, pp. 163-179, (2008).

[31] K. Hajebi and J. S. Zelek, "Structure from Infrared Stereo Images," in Canadian Conference on Computer and Robot Vision, Waterloo, Ontario, Canada, pp. 105-112, (2008).

[32] M. A. Ordal, L. L. Long, R. J. Bell, R. R. Bell, R. W. Alexander, and C. A. Ward, "Optical properties of the metals Al, Co, Cu, Au, Fe, Pb, Ni, Pd, Pt, Ag, TI, and W in the infrared and far infrared," Applied Optics, vol. 22, no. 7, (Avril 1983).

[33] Edward D. Palik, Handbook of Optical Constants of Solids. Boston: Academic Press, (1985).

[34] F. Marzani, Y. Voisin, L. F. C. Lew Yan Voon, and A. Diou, "Calibration of a three-dimensional reconstruction system using a structured light source," Optical Engineering, vol. 41, no. 2, pp. 484-492, (2002).

[35] A. Bajard, O. Aubreton, Y. Bokhabrine, B. Verney, G. Eren, A. Ercil, and F. Truchetet, "Three-dimensional scanning of specular and diffuse metallic surfaces using an infrared technique," Optical Engineering, vol. 51, no. 06, (June 2012).

[36] G. Eren, "3D Scanning of Transparent objects," Université de Bourgogne - Sabancı Üniversitesi, PhD thesis, (September 2010).

[37] B. K. P. Horn." Shape from Shading: A Method for Obtaining the Shape of a Smooth Opaque Object from One View", PhD thesis, MIT, (1970).

[38] D. Miyazaki, M. Kagesawa, and K. Ikeuchi, "Determining Shapes of Transparent Objects from Two Polarization Images," in IAPR, pp. 26-31, (2002)

[39] D. Miyazaki, M. Saito, Y. Sato, and K. Ikecuhi, "Determining Surface Orientations of transparent objects on polarization degrees in visible and infrared wavelength," J. Opt. Soc. Am. A, Vol. 19, pp. 687-694, (2002).

[40] D. Miyazaki and K. Ikeuchi, "Shape Estimation of Transparent Objects by Using Inverse Polarization Ray Tracing," IEEE Trans. On Pattern Analysis and Machine Intelligence, Vol. 29,pp. 2018-2030, (2007).

[41] S. J. Tyo, D. L. Goldstein, D. B. Chenault, and J. A. Shaw, "Review of passive imaging polarimetry for remote sensing applications," Appl. Opt. , Vol 45, pp. 5453-5469, (2006).

[42] D. L. Goldstein, Polarized light second Edition (Optical Engineering), p. 680, (2003).

[43] M. Born and E. Wolf. Principles Of Optics. Cambridge, 7 edition, (1999).

[44] R. Seulin, F. Merienne, and P. Gorria. Simulation of specular surface imaging based on computer graphics : application on a vision inspection system. EURASIP Journal on Applied Signal Processing, 2002(7):649–658, (July 2002).

[45] D. Miyazaki, M. Kagesawa, and K. Ikeuchi, "Polarization-based transparent surface modeling from two views," in International Conference on Computer Vision, 2003).

[46] C. Stolz, M. Ferraton and F. Mériaudeau, " Shape from polarization: a method for solving zenithal angle ambiguity," Optics Letters, (2012, in revision).

[47] F. Meriaudeau, R. Rantoson , K. Adal., C. Stolz, "shape from polarization in the far IR, application to 3D digitization of transparent objects", submitted to Optics Letters.